Title: Weakly hydrated anions bind to polymers but not monomers in aqueous solutions

Author List: Bradley A. Rogers[1], Halil I. Okur[1#], Chuanyu Yan[1], Tinglu Yang[1], Jan Heyda[3], Paul S. Cremer[1,2*]

Affiliations:

[1]Department of Chemistry, The Pennsylvania State University, University Park, Pennsylvania 16802.

[2]Department of Biochemistry and Molecular Biology, The Pennsylvania State University, University Park, Pennsylvania 16802.

[3]Department of Physical Chemistry, University of Chemistry and Technology, Prague, Technicka 5 16628, Prague 6 - Dejvice, Czech Republic

[#]The current address for H.I.O. is Department of Chemistry and National Nanotechnology Research Center (UNAM), Bilkent University, 06800 Ankara, Turkey

Contact Information: *Corresponding Author: psc11@psu.edu

Abstract:

Weakly hydrated anions help to solubilize hydrophobic macromolecules in aqueous solutions, but small molecules comprised of the same chemical constituents precipitate out when exposed to these ions. Herein, this apparent contradiction is resolved by systematically investigating the interactions of NaSCN with polyethylene oxide oligomers and polymers of varying molecular weight. A combination of spectroscopic and computational results reveals that SCN^- accumulates near the surface of polymers, but is excluded from monomers. This occurs because SCN^- preferentially binds to the center of macromolecular chains, where the local water hydrogen bonding network is disrupted. These findings suggest a link between ion-specific effects and theories addressing how hydrophobic hydration is modulated by the size and shape of a hydrophobic entity.

Main Text:

Weakly hydrated anions, such as I^-, SCN^-, and ClO_4^-, weaken the hydrophobic effect in aqueous solutions. These large, polarizable anions denature proteins, inhibit supramolecular complexation, and dissolve surfactant micelles [1–3]. At the molecular level, weakly hydrated anions partially shed their hydration shells and adsorb to nonpolar interfaces, thereby inhibiting hydrophobic assembly [4–10]. The adsorption of these anions to amide-rich polymers has been characterized by sub-molar to molar equilibrium dissociation constants, K_D = 0.05-1.60 M [11–14]. Even tighter adsorption has been observed at macroscopic surfaces, such as the air/water interface, K_D = 0.03-0.26 M, and in the concave pockets of cavitands and proteins, K_D = 0.003-0.09 M [2,15–22]. By stark contrast, anions are repelled from small molecules, like *N*-methyl acetamide and tert-butyl alcohol, K_D = 4-8 M [23,24]. As a consequence, weakly hydrated anions precipitate small non-ionic solutes out of aqueous solutions, including acetone and diacetone alcohol [25]. The dramatic range of anion affinity for chemically similar aliphatic binding sites exposes a critical gap in our knowledge of the mechanisms for anion-specific effects.

The surface curvature of nonpolar solutes is known to influence solubility because of the distinct local hydration of curved and flat interfaces [26,27]. The water hydrogen bonding network can wrap around small and convex solutes to maintain its bulk-like structure. Large solutes, however, have a flatter topography that disrupts the hydrogen bonds between water molecules [27]. As such, small solutes can be incorporated into the water network, while larger ones with broken hydrogen bonds associate with each other and release water molecules into the bulk solution. The cartoon in Figure 1 depicts a simple model for a polymer chain. The termini are highly curved due to their half spherical geometry, while the center of the chain is flatter because it has cylindrical-like structure. Experimental and computational studies of nonpolar solutes with varying chain lengths have shown that this topography disorders water at the center of the chain more than at the termini [28,29].

Herein, the role of surface curvature on anion-specific effects is explored by systematically measuring the interactions of NaSCN with polyethylene oxides of varying molecular weights, ranging from monomers to polymers. The results indicate that SCN^- is repelled from monomers but attracted to oligomers of increasing chain length. These interactions are distinct because SCN^- binds selectively to the center of oligomer chains, as opposed to their termini (Figure 1). Investigations of polyether hydration shells reveal that the water structure at the center of the chain is more disordered than at the termini. Together, these findings imply that SCN^- interacts with low curvature interfaces to displace water at sites of hydrogen bonding defects. The correlation of binding affinity and water structure measurements at specific locations along the polyether solutes establishes a link between ion-specific effects (Hofmeister series chemistry) and the hydration of hydrophobic interfaces.

Results

Heterogeneous Adsorption of Weakly Hydrated Anions to Polyether Chains

The adsorption of NaSCN to PEO-5 was monitored by ^{1}H nuclear magnetic resonance (NMR) spectroscopy. The nature of the interaction was determined from changes in the solute's proton chemical shifts, $\Delta\delta$, at a given salt concentration, c_{salt}. The four spectrally unique proton positions for PEO-5 are denoted Central, Penultimate, End and Termini in Figure 2a. The chemical shift values associated with the terminal methyl protons (blue data points) and internal methylene protons (red, orange and green data points) decrease upon the introduction of NaSCN (Figure 2b). The decrease at the termini is linear with a slope value, a, as modeled by the first term in equation (1). By contrast, data from the internal methylene groups displays non-linear behavior below 0.1 M NaSCN. The non-linearity can be fit to a Langmuir binding isotherm as defined by the second term in equation (1). This non-linear term corresponds to the small, saturable increase in the chemical shift, δ_{max}, as SCN^- binds to the chain. The binding strength at the internal methylene groups can be quantified by a sub-molar equilibrium dissociation constant, K_D = 0.1 M. The value of K_D at the termini, however, is too weak to be detected, $K_D > 2.4$ M.

$$\Delta\delta = ac_{\text{salt}} + \frac{\delta_{\max} c_{\text{salt}}}{K_D + c_{\text{salt}}} \qquad \text{Equation (1)}$$

The free energy of adsorption, i.e. $\Delta G_{ads} = RT \ln(K_D)$, is plotted for specific positions on the PEO-5 chain in Figure 2c (open data points). Positive values of ΔG_{ads} indicate repulsion of NaSCN, while negative values denote attraction. As can be seen, SCN^- was repelled from the methyl termini, but attracted to the methylenes along the interior of the chain. Figure 2c also includes the average values for ΔG_{ads} (filled data points) obtained from analogous NMR experiments that were performed on a large set of polyethers with different chain lengths. The chain lengths ranged from the monomer to a 20,000-mer, as illustrated in Figure 2d. These results indicate that salt ions were repelled from the methyl termini and attracted to the center of the chain, regardless of chain length.

All-atom molecular dynamics (MD) simulations of PEO-5 in NaSCN solutions also revealed heterogeneous adsorption of the salt ions. The interaction between the ions and the solute was quantified by the preferential interaction coefficient, Γ_{23}, where water, solute, and salt are designated by the indices 1, 2 and 3, respectively [30]. Positive values of Γ_{23} represent an accumulation of NaSCN relative to the bulk concentration, whereas negative values denote depletion. The values of Γ_{23} were normalized to both the salt concentration and the solvent accessible surface area (*SASA*) and referred to as μ_{23} [31]. The μ_{23} data are organized by position along the PEO-5 chain in Figure 2e (open data points). The average values of μ_{23}, which were obtained from MD simulations of different polyethers of varying chain length, are also provided in Figure 2e (filled data points). As can be seen, salt ions accumulate near the internal aliphatic moieties and are slightly depleted from the terminal methyl groups.

Collectively, these results suggest that the adsorption of SCN^- to the polyether chain is heterogeneous, with tighter binding at the center of the chain and weaker interactions near the termini. This is the case despite the fact that the monomer chemistry is essentially identical at each position. Such findings imply

that the tighter affinity to long chains occurs because the concentration of the termini is diluted with increasing chain length. Moreover, these studies are consistent with a surface curvature hypothesis. Namely, the binding affinity appears to correlate with the lower curvature at the cylindrical center of the chains, as opposed to the half spherical terminal segments, which exhibit higher curvature (Figure 1).

Structure of Water in Polyether Hydration Shells

The mechanism depicted in Figure 1 suggests that the adsorption of weakly hydrated anions to polymer interfaces may be controlled by the differences in hydration of the center and termini moieties of the chain. As such, Raman-multivariate curve resolution (Raman-MCR) spectroscopy was employed to probe the structure of the polyether hydration shells in neat water [32]. MCR analysis allows the Raman spectrum of a solution to be separated into two components that correspond to the solute hydration shell and the bulk water, as depicted schematically in Figure 3a. The distinction between these two regions is illustrated by the dashed black outline around the polymer chain. The hydration shell spectra of PEO-1 and PEO-2,000 are shown in Figure 3b. Both spectra display a broad OH stretch peak between 3000 to 3600 cm^{-1} that reports on water molecules in the hydration shell. The solid blue and red lines in Figure 3b are fits to the data using two Gaussian peaks for the OH stretch region. The peak at 3250 cm^{-1} (vertical dashed blue line) can be assigned to more tetrahedrally ordered water molecules, while the peak near 3450 cm^{-1} (vertical dashed red line) is attributed to water molecules with weaker and less tetrahedral hydrogen bonds [33–37].

The area ratio of the 3250 cm^{-1} peak to the 3450 cm^{-1} peak, A_{3250}/A_{3450} , can be used as a metric for the structure of water around a given chain, with higher values corresponding to increased ordering. Raman-MCR measurements for the entire set of polyethers reveal a chain length dependence to the A_{3250}/A_{3450} value (Figure 3c). As can be seen, the value of A_{3250}/A_{3450} decreases with chain length implying a disruption of the tetrahedral water structure at the center of the chain. Indeed, the hydration shells of longer chains should be dominated by water molecules solvating central groups, rather than the termini,

since they constitute most of the solvent accessible surface area, *SASA*. The black curve in Figure 3c is a fit to the data using a segmented chain model, where the total value of A_{3250}/A_{3450} is calculated as the linear combination of the segment-specific ratios, $(A_{3250}/A_{3450})_i$, that are weighted by their fraction of the *SASA*. Four segments were used in the fit based on the binding sites observed in the NMR experiments (Figure 2).

The structure of water in the MD simulations can be quantified by the tetrahedral order parameter, q [38]. Water molecules in ideal tetrahedral hydrogen bonding geometries yield a q value of 1, while random geometries, akin to an ideal gas, give rise to $q = 0$. The probability distribution of the tetrahedral order parameter, $P(q)$, for the terminal (blue) and center (red) segments of the PEO-5 hydration shell as well as bulk water (black) are plotted in Figure 3d. As can be seen, the probability of observing more tetrahedral hydrogen bonding, $P(0.76)$, is higher in bulk water than in the vicinity of the methyl termini (vertical dashed blue line). Moreover, the water structure is even more disordered adjacent to the central groups (vertical dashed red line). The values of $P(0.76)$ relative to the respective bulk water values are plotted for each of the four segments of PEO-5 in Figure 3e (open data points) along with the average results from simulations of polyethers ranging from the monomer to a 35-mer (closed data points). As can be seen, the changes in interfacial water structure at specific sites along the polyether chains (Figure 3e) corresponds to the anion binding interactions (Figures 2c and 2e). This idea is depicted schematically in Figure 3a as the ordered and disordered water structures.

Correlation of Binding Affinity and Water Structure

The adsorption of NaSCN to a specific position on the polyether chain reflects the degree of order in the hydration shell at that site. This relationship is quantified in Figure 4a, which plots the adsorption free energies as measured by NMR (Figure 2c) against the segment-specific ratios of the Raman OH stretch bands (Figure 3c). An analogous correlation from the simulation studies is shown in Figure 4b to relate the normalized preferential interaction coefficient (Figure 2e) to the probability of forming water

networks with more tetrahedral order (Figure 3e). The consequences of this relationship are apparent in the ion density map shown in Figure 4c. Hot spots for SCN^- adsorption occur along the middle of the PEO-5 chain (yellow isobars), while Na^+ binding is localized to the ether oxygens (green isobars). Significantly, the SCN^- binding sites match the water structure heat map in Figure 4d that depicts the value of P/P_{bulk} (q = 0.76) for water molecules solvating specific heavy atoms along the chain. The heavy atoms are colored blue where the value of P/P_{bulk} is high, indicating an ordered solvation shell, and red where the value is low, denoting disordered hydration. Together, these results demonstrate that broken hydrogen bonds in the hydration shells at the polymer's center are more readily displaced by weakly hydrated anions compared to the termini (Figure 1). On the other hand, the more tetrahedrally ordered hydration shells of the monomer and the polymer's termini appear to inhibit the adsorption of SCN^-.

Discussion

In this work, the concept of molecular surface curvature is employed to explain the correlation between interfacial water structure and the binding of Hofmeister anions. The systematic investigation of chain length effects on SCN^- adsorption and water structure reveals distinct behaviors at the methyl termini and the internal methylene moieties along the chain. Location-specific analysis is consistent with the idea that the center of the chain resembles a cylinder-like structure, while the termini are reminiscent of half spheres (Figure 1). Water is more tetrahedrally ordered near the latter regions. By contrast, along the center of the chain, there are weaker and less tetrahedral hydrogen bonds. It is at these sites of disordered hydrogen bonding where the strongest affinity for SCN^- occurs. The correlation in Figure 4 provides a systematic depiction of the ability for water structure to completely reverse the nature of the interactions of weakly hydrated anions with nonpolar surfaces, i.e. ΔG_{ads} varies from -5.3 to > +2.2 kJ mol^{-1} (K_D = 0.1 to > 2.4 M).

The relationship between surface curvature and interfacial water structure is central to the hydrophobic effect. Small and convex aliphatic molecules are significantly more soluble than their larger and flatter

counterparts, despite their chemical similarity [39,40]. Stillinger envisioned that bulk-like hydrogen bonding of water would be preserved around small solutes, but disrupted near the surfaces of large solutes, which more closely resemble the air/water interface [26]. Quantitative theories and computer simulations predict a crossover between these two regimes at nanometer length scales [41,42]. Simulations and spectroscopy experiments have observed signatures of this crossover in the dynamics of water at interfaces with varying curvature [43–45]. The hydration of *n*-alcohols as a function of chain length and the solvation free energy of polymers with differently sized aromatic side chains both exhibit signatures of the predicted crossover length scale [28,46]. The distance between the termini and end group methylenes of the polyethers investigated in this work is ~ 0.5 nm, which is very close to the characteristic crossover length for water structure and hydrophobicity [27,28,42]. As such, the internal segments of the chain behave like surfaces with reduced curvature, which create water structure defects that are readily displaced by weakly hydrated anions.

The chain length dependence and site specificity of anion adsorption and hydration structure is not limited to NaSCN and polyethylene oxides. As discussed in Sections 2 and 5 of the *Supplementary Information* (Supplementary Figures 23-31 and 57-59), these effects apply to other weakly hydrated anions, like I^-, and polymers, such as polyacrylamides. Moreover, the results are similar when other alkali metal cations are employed, like Li^+ and Cs^+. Despite their chemical differences, this simple model invoking surface curvature predicts how anion-specific interactions vary with binding site location and chain length. The bifurcation in anion-hydrophobic interactions leads to divergent macroscopic behavior for small molecules and polymers. Indeed, weakly hydrated anions reduce the solubility of small molecules in aqueous solutions, but inhibit the hydrophobic collapse of thermoresponsive polymers and denature proteins [1,11,25,47]. The incorporation of local surface curvature concepts into theoretical models should improve predictions for anion-specific effects on both small molecules and protein macromolecules. In a broader sense, the binding of anions as a function of molecular surface curvature should impact a variety

of phenomenon involving hydrophobic interfaces, ranging from the formation of methane clathrates to host-guest supramolecular complexation.

Figure and Captions:

Figure 1. Schematic diagram of a polymer chain and the effects its surface curvature have on interfacial water structure and SCN^- adsorption. The hydration shell is well-ordered near the curved termini, which leads to the exclusion of SCN^- (blue region). By contrast, SCN^- readily adsorbs to the center of the chain because the water is more disordered by its flatter surface curvature (red region).

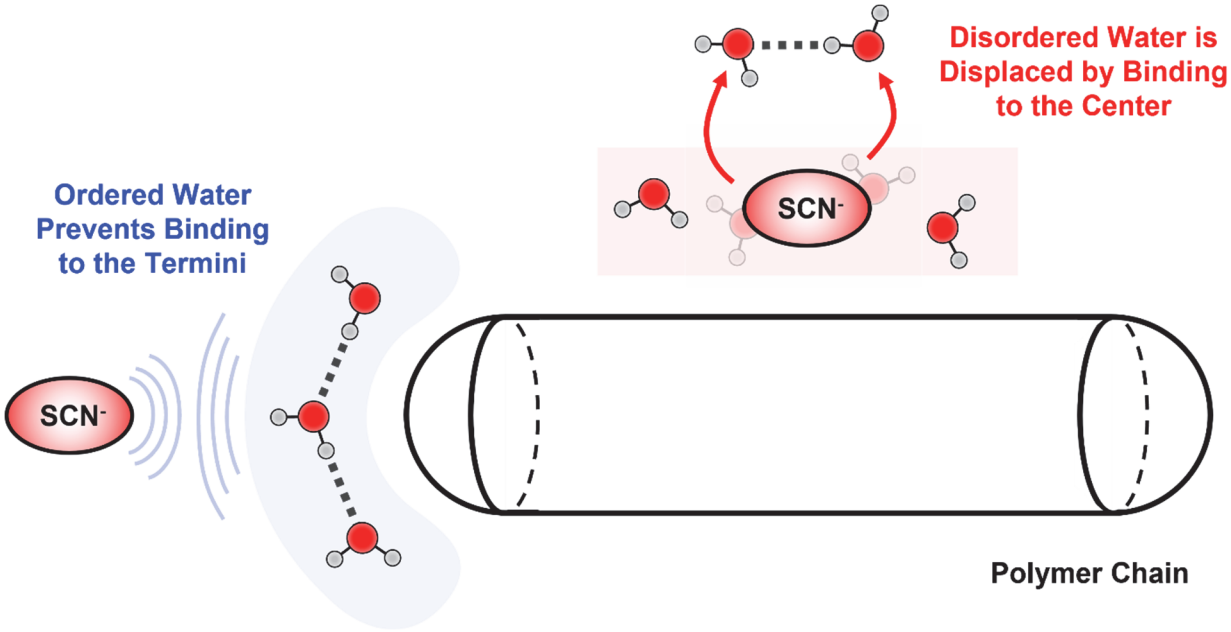

Figure 2. The interaction of NaSCN with polyethers. (a) Schematic illustration of SCN^- binding to the center of PEO-5, but not to its termini. (b) Salt-induced ^1H NMR chemical shifts, $\Delta\delta$, are used probe the interactions of SCN^- with the central (red), penultimate (orange), and end (green) methylenes as well as terminal methyl groups (blue) of PEO-5. The solid lines are fits to equation 1. The error bars represent the standard deviation of 2-3 solution preparations and are smaller than most of the data points. (c) The free energy of NaSCN adsorption, ΔG_{ads}, for the individual segments of PEO-5 (open) quantify the heterogenous adsorption of SCN^- to the chain. The average ΔG_{ads} values (filled) for these segments are obtained from multiple PEOs (1, 2, 3, 4, 5, 2,000, 20,000) and PEGs (6, 8, 35, 75, 227). The error bars for PEO-5 are the standard deviation of 2 NaSCN titrations, while the error bars for the average values are obtained by error propagation calculations. The blue arrow denotes that ΔG_{ads} is weaker than the limit of detection at the chain's termini. The minimum and maximum estimates for the limit of detection are represented by the blue error bars. (d) Structures of various PEOs illustrate the chain length dependence of the NaSCN binding site specificity. (e) The preferential interaction coefficient, μ_{23}, for the individual segments of PEO-5 (open) and averages (filled) are obtained from simulations for various PEOs (1, 3, 5, 7, 14, 35) and support the NMR results. The error bars are the standard error of the mean for each segment in the simulation. The NMR experiments, MD simulations and the role of cation and anion identity are described in Sections 1 and 2 of the *Supplementary Information* (Supplementary Figures 1-40).

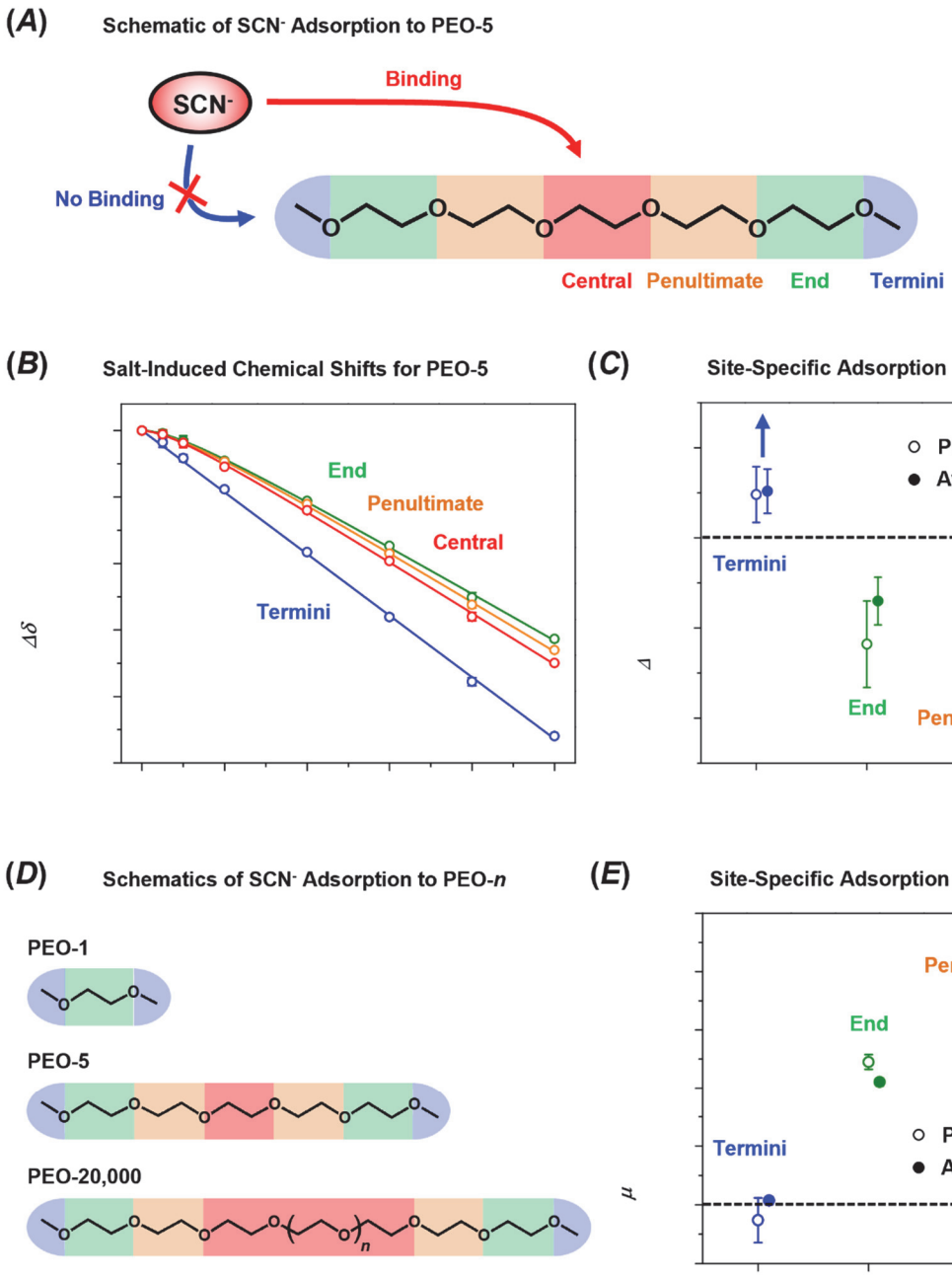
(A)
Schematic of SCN- Adsorption to PEO-5
SCN-
Binding
No Binding
Central
Penultimate
End
Termini
(B)
Salt-Induced Chemical Shifts for PEO-5
End
Penultimate
Central
Termini
Δδ
(C)
Site-Specific Adsorption by NMR
PEO-5
Average for PEO-n
Termini
End
Penultimate
Central
Δ
(D)
Schematics of SCN- Adsorption to PEO-n
PEO-1
PEO-5
PEO-20,000
(E)
Site-Specific Adsorption by MD
Central
Penultimate
End
Termini
PEO-5
Average for PEO-n
μ

1

2

3

4

Figure 3. Structure of water in polyether hydration shells. (a) Schematic illustration of PEO-5 hydration, where the hydrogen bonded network of water is more ordered at the termini (blue region) than at the center of the chain (red region). (b) Hydration shell spectra of PEO-1 (blue) and PEO-2,000 (red) obtained by Raman spectroscopy and multivariate curve resolution analysis. The solid curves represent fits to the data using a sum of Gaussian peaks. As the chain length is increased, the intensity of the peak corresponding to tetrahedrally ordered water (3250 cm^{-1}, dashed blue line) decreases relative to the disordered water peak (3450 cm^{-1}, dashed red line). (c) The area ratio of these two peaks, A_{3250}/A_{3450}, shows the chain length induced structural transformation of the polyether hydration shell. The error bars are the standard deviation of 3 solution preparations. The solid curve is the best fit of the data to a segmented chain model, which quantifies the values of A_{3250}/A_{3450} for each segment of the chain. (d) The probability distribution of the tetrahedral order parameter, $P(q)$, for bulk water (black data) versus water hydrating the termini (blue data) and center (red data) of PEO-5. Water molecules in tetrahedrally ordered hydrogen bonding networks ($q = 0.76$, dashed blue line) are less populated at the center of the chain than at the termini. (e) The probability of observing tetrahedrally ordered water in the polyether hydration shell relative to the bulk solution, P/P_{bulk} ($q = 0.76$), for each segment of PEO-5 (open). The average values (filled) are obtained from simulations of the same solutes described in Figure 2. The error bars are the standard error of the mean for each segment in the simulation. The Raman-MCR experiments and q computations are described in Section 3 of the *Supplementary Information* (Supplementary Figures 41-54).

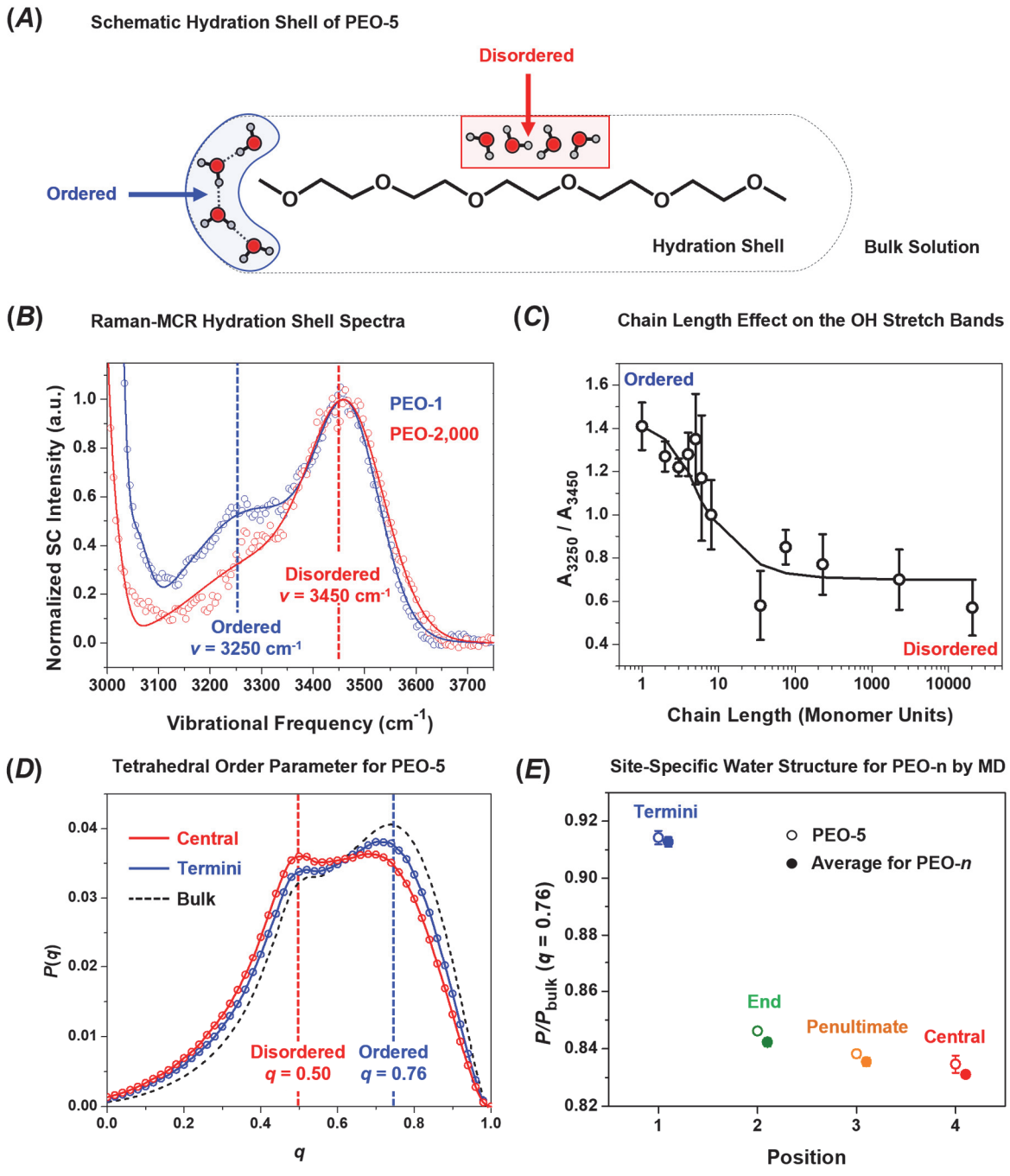
(A)
Schematic Hydration Shell of PEO-5
Disordered
Ordered
Hydration Shell
Bulk Solution
(B)
Raman-MCR Hydration Shell Spectra
Normalized SC Intensity (a.u.)
PEO-1
PEO-2,000
Disordered
ν = 3450 cm-1
Ordered
ν = 3250 cm-1
Vibrational Frequency (cm-1)
(C)
Chain Length Effect on the OH Stretch Bands
A3250 / A3450
Ordered
Disordered
Chain Length (Monomer Units)
(D)
Tetrahedral Order Parameter for PEO-5
P(q)
Central
Termini
Bulk
Disordered
q = 0.50
Ordered
q = 0.76
q
(E)
Site-Specific Water Structure for PEO-n by MD
P/Pbulk (q = 0.76)
Termini
PEO-5
Average for PEO-n
End
Penultimate
Central
Position

1

2

Figure 4. The role of interfacial water structure on NaSCN adsorption to polyether chains. (a) Correlation of the free energy of NaSCN adsorption, ΔG_{ads}, and the ratio of ordered to disordered water in the hydration shell, A_{3250}/A_{3450}. (b) Correlation of the NaSCN preferential interaction coefficient, μ_{23}, versus the probability of observing tetrahedrally ordered water in the hydration shell, P/P_{bulk} (q = 0.76). The data points in (a) and (b) represent the average values for each segment of the polyether chains described in Figures 2 and 3. The error bars in (a) and (b) are the standard deviation and standard error of the mean, respectively. The strong correlations observed in both the experiments and simulations suggest that the adsorption of NaSCN to the interior segments of the polyether chains is enhanced by the displacement of disordered water structures from the polyether hydration shell. (c) The NaSCN density map shows the heterogenous accumulation of ions around the PEO-5 chain. The opaque and transparent clouds represent isosurfaces where SCN^- (yellow) or Na^+ (green) is 6 or 3 times the bulk density, respectively. (d) The heat map of the P/P_{bulk} (q = 0.76) values depicts the distinct tetrahedral structure of water at the center and termini of the PEO-5 hydration shell. Each heavy atom is colored according to the scale that is provided as an inset. The correspondence of the SCN^- accumulation in (c) with the tetrahedral water structure in (d) provides a visual representation of the site-specific correlations in (a) and (b). Further discussion of the correlations is provided in Section 4 of the *Supplementary Information* (Supplementary Figures 55-56).

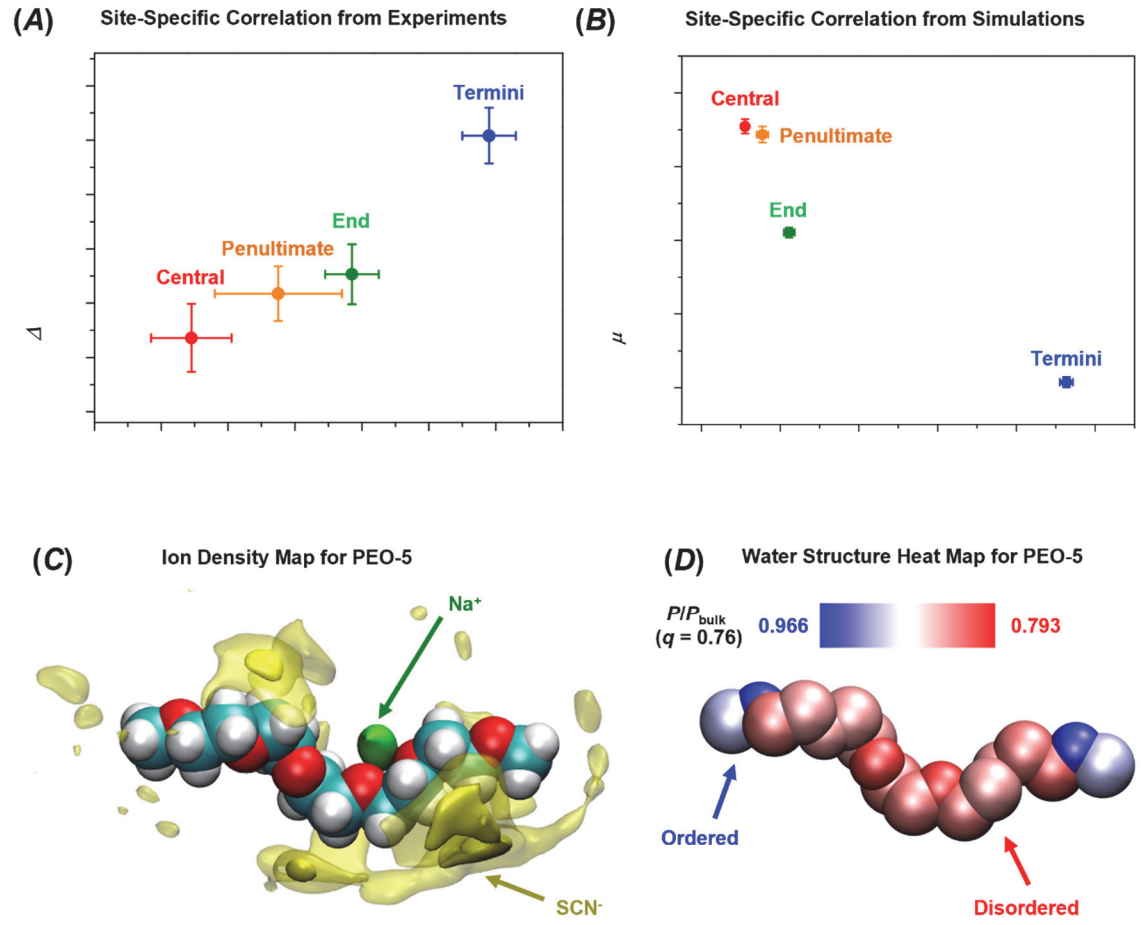
(A)
Site-Specific Correlation from Experiments
Termini
End
Penultimate
Central
Δ
(B)
Site-Specific Correlation from Simulations
Central
Penultimate
End
Termini
μ
(C)
Ion Density Map for PEO-5
Na+
SCN-
(D)
Water Structure Heat Map for PEO-5
P/P bulk
(q = 0.76)
0.966
0.793
Ordered
Disordered

1

2

Methods:

Reagents. High purity sodium thiocyanate was used in all experiments (NaSCN, 99.99%). The monomer and oligomers of polyethylene glycols (PEG-*n*) were liquids and at least 95% pure: ethylene glycol (PEG-1, 99.8%), diethylene glycol (PEG-2, ≥99.0%,), triethylene glycol (PEG-3, 99%), tetraethylene glycol (PEG-4, 99%), pentaethylene glycol (PEG-5, 98%), hexaethylene glycol (PEG-6, 97%), octaethylene glycol (PEG-8, ≥95%). The monomer and oligomers of polyethylene oxide (PEO-*n*) were also liquids with at least 99% purity: 1,2-dimethoxyethane (PEO-1, 99.9%), diethylene glycol dimethyl ether (PEO-2, 99.5%), Triethylene glycol dimethyl ether (PEO-3, 99%), tetraethylene glycol dimethyl ether (PEO-4, ≥99%), polyethylene glycol dimethyl ether M_n ~ 250 (PEO-5, n20/D 1.441). The longer chain PEGs and PEOs were solid powders: polyethylene glycol M_w ~ 1,500 (PEG-35), polyethylene glycol M_w ~ 3,350 (PEG-75), polyethylene glycol M_w ~ 10,000 (PEG-227), polyethylene oxide M_v ~ 100,000 (PEO-2k), and polyethylene oxide M_v ~ 900,000 (PEO-20k).

Sample Preparation. NaSCN was dried at 115 °C for 8 hours prior to preparing solutions to remove adsorbed water. All solutions were prepared using 18 MΩ-cm deionized water. The stock salt solutions were prepared gravimetrically in volumetric flasks. The stock polyether solutions for the liquid polyethers were prepared volumetrically by diluting a volume of the pure liquid with water. Stock polyether solutions of the solid PEGs were prepared gravimetrically. The salt and polyether stock solutions were mixed volumetrically with water to prepare the ternary solutions. The final monomer concentration was 0.25 M (~5 mg/mL) for all chain lengths. The volumes were assumed to be additive.

NMR Spectroscopy. ^{1}H NMR experiments were performed with precision coaxial insert NMR tubes. The external reference, 2 mg/mL 4,4-dimethyl-4-silapentane-1-sulfonic acid, and the locking agent, deuterium oxide, were loaded into a coaxial insert. The insert was then positioned in the center of a 5 mm precision sample tube. The spectra were collected on a 500 MHz spectrometer. After the samples were equilibrated to 298 K for 2 minutes, one-dimensional ^{1}H spectra were acquired using Bruker's standard

excitation sculpting for water suppression [48]. Additional details for the NMR instrumentation, pulse sequence and data analysis are described in the *Supplementary Information*.

Raman Spectroscopy. Raman spectra were collected on a home-built instrument. The 514.5 nm line of a mixed Ar-Kr gas laser was focused to the center of a 1 cm quartz cuvette. The unpolarized Raman signal was collected in a backscattering geometry and directed to a spectrometer. The power of the incident light at the sample was adjusted to 50 mW and the collection time was 5 min. The solutions contained 0.5 M monomer concentration (~11 mg/mL) for all chain lengths. Hydration shell spectra were extracted using a multivariate curve resolution (MCR) algorithm written for IGOR Pro by Prof. Dor Ben-Amotz at Purdue University. The inputs for the MCR analysis were a spectrum of an aqueous solution containing a polyether and a spectrum of pure water. The output was the deconvolution of the solution spectrum into components for pure water and another for the hydration shell. An extended discussion of the spectrometer design and MCR analysis is provided in the *Supplementary Information*.

Simulation Composition. All-atom molecular dynamics (MD) studies were performed with polyether chains that were 1, 3, 5, 7, 14, or 35 monomer units long [49,50]. Each simulation involved 3100-3400 water molecules (SPC/E) and the number of chains was adjusted to mimic the constant monomer concentration employed in the experiments [51]. All simulation boxes reached an approximate volume of 4.7x4.7x4.7 nm^3 after an initial *NpT* equilibration (20 ns). The evaluation of water structure was conducted on MD simulations containing only 1 polymer chain to avoid the potential bias from chain-chain interactions. The ion-polymer interactions were evaluated from simulations of 1 M salt solution that were parameterized using non-polarizable force fields for the ions [13,52,53]. The polymers were flexible in all of the simulations, except simulations that were performed to create the three-dimensional density maps, where the polymer was constrained to the average conformation.

Simulation Algorithms and Data Analysis. Simulations were carried out over several hundred ns with a time step of 2 fs with the GROMACS simulation package [54]. Trajectories were stored at 1 ps intervals, resulting in 10^5-10^6 samples for subsequent data analysis. The systems were constrained to 300 K and 1 atm using a velocity-rescale for canonical sampling thermostat and Parrinello-Rahman barostat with coupling constants of 0.1 and 2 ps, respectively [55,56]. Three-dimensional periodic boundary conditions were applied. Long-range electrostatic interactions beyond the nonbonded cutoff of 10 Å were accounted for using the particle mesh Ewald method on a 0.16 nm grid [57]. All bonds containing hydrogen atoms were constrained using the LINCS algorithm [58]. Preferential binding of ions to the polyether surfaces was calculated by means of Kirkwood-Buff theory [30,59]. Water structure was evaluated using the tetrahedral order parameter [60,38].

Acknowledgements:

The authors thank Chen Chen, Zhicheng Tian and Harry Allcock for PDEA synthesis (The Pennsylvania State University), Tapas Mal and Carlos Pacheco for NMR assistance, as well as Dor Ben-Amotz and Will Noid for insightful discussions. **Funding:** PSC thanks the National Science Foundation (CHE-2004050) for support. JH thanks the Czech Science Foundation (grant 20-24155S) and the Ministry of Education, Youth and Sports of the Czech Republic through the e-INFRA CZ (ID:90140).

Author Contributions:

The project and mechanism were conceptualized by BAR, HIO, and PSC. The work was designed and the methods were developed with the help of all authors (BAR, HIO, CY, TY, JH, and PSC). Experimental data was acquired and analyzed by BAR, HIO, and CY, while JH ran, analyzed and wrote software algorithms for the computer simulations. BAR, HIO, CY, JH, and PSC interpreted the data. The original draft was written by BAR, HIO, and PSC. The manuscript was revised and edited by BAR, HIO, JH and PSC.

Competing Interests:

The authors have no competing interests.

Data and Materials Availability:

The datasets generated during and/or analyzed during the current study are available in the Source Data files and Supplementary Data files. The DOIs for these files are listed below.

Figure 2: 10.5281/zenodo.5123016

Figure 3: 10.5281/zenodo.5123100

Figure 4: 10.5281/zenodo.5123104

Supplementary Figures: 10.5281/zenodo.5123295

Code Availability:

The codes and algorithms generated during the current study are available from the corresponding author on reasonable request.

References:

1. Bye, J. W. & Falconer, R. J. Thermal Stability of Lysozyme as a Function of Ion Concentration: A Reappraisal of the Relationship between the Hofmeister Series and Protein Stability. *Protein Sci.* **22**, 1563–1570 (2013).
2. Gibb, C. L. D. & Gibb, B. C. Anion Binding to Hydrophobic Concavity Is Central to the Salting-in Effects of Hofmeister Chaotropes. *J. Am. Chem. Soc.* **133**, 7344–7347 (2011).
3. Ray, A. & Nemethy, G. Effects of Ionic Protein Denaturants on Micelle Formation by Nonionic Detergents. *J. Am. Chem. Soc.* **93**, 6787–6793 (1971).
4. Zhang, Y. & Cremer, P. S. Interactions between Macromolecules and Ions: the Hofmeister Series. *Curr. Opin. Chem. Biol.* **10**, 658–663 (2006).
5. Petersen, P. B. & Saykally, R. J. On the Nature of Ions at the Liquid Water Surface. *Annu. Rev. Phys. Chem.* **57**, 333–364 (2006).
6. Tobias, D. J. & Hemminger, J. C. Getting Specific about Specific Ion Effects. *Science* **319**, 1197–1198 (2008).
7. Pegram, L. M. & Record, M. T. Thermodynamic Origin of Hofmeister Ion Effects. *J. Phys. Chem. B* **112**, 9428–9436 (2008).
8. Zhang, Y. & Cremer, P. S. Chemistry of Hofmeister Anions and Osmolytes. *Annu. Rev. Phys. Chem.* **61**, 63–83 (2010).
9. Lo Nostro, P. & Ninham, B. W. Hofmeister Phenomena: An Update on Ion Specificity in Biology. *Chem. Rev.* **112**, 2286–2322 (2012).
10. Okur, H. I. *et al.* Beyond the Hofmeister Series: Ion-Specific Effects on Proteins and Their Biological Functions. *J. Phys. Chem. B* **121**, 1997–2014 (2017).
11. Zhang, Y., Furyk, S., Bergbreiter, D. E. & Cremer, P. S. Specific Ion Effects on the Water Solubility of Macromolecules: PNIPAM and the Hofmeister Series. *J. Am. Chem. Soc.* **127**, 14505–14510 (2005).

12. Cho, Y. *et al.* Effects of Hofmeister Anions on the Phase Transition Temperature of Elastin-like Polypeptides. *J. Phys. Chem. B* **112**, 13765–13771 (2008).
13. Rembert, K. B. *et al.* Molecular Mechanisms of Ion-Specific Effects on Proteins. *J. Am. Chem. Soc.* **134**, 10039–10046 (2012).
14. Rembert, K. B., Okur, H. I., Hilty, C. & Cremer, P. S. An NH Moiety Is Not Required for Anion Binding to Amides in Aqueous Solution. *Langmuir* **31**, 3459–3464 (2015).
15. Dang, L. X. Computational Study of Ion Binding to the Liquid Interface of Water. *J. Phys. Chem. B* **106**, 10388–10394 (2002).
16. Jungwirth, P. & Tobias, D. J. Ions at the Air/Water Interface. *J. Phys. Chem. B* **106**, 6361–6373 (2002).
17. Petersen, P. B., Saykally, R. J., Mucha, M. & Jungwirth, P. Enhanced Concentration of Polarizable Anions at the Liquid Water Surface: SHG Spectroscopy and MD Simulations of Sodium Thiocyanide. *J. Phys. Chem. B* **109**, 10915–10921 (2005).
18. Otten, D. E., Shaffer, P. R., Geissler, P. L. & Saykally, R. J. Elucidating the Mechanism of Selective Ion Adsorption to the Liquid Water Surface. *Proc. Natl. Acad. Sci. U.S.A.* **109**, 701–705 (2012).
19. Fox, J. M. *et al.* Interactions between Hofmeister Anions and the Binding Pocket of a Protein. *J. Am. Chem. Soc.* **137**, 3859–3866 (2015).
20. McCaffrey, D. L. *et al.* Mechanism of Ion Adsorption to Aqueous Interfaces: Graphene/Water vs. Air/Water. *Proc. Natl. Acad. Sci. U.S.A.* **114**, 13369–13373 (2017).
21. Sokkalingam, P., Shraberg, J., Rick, S. W. & Gibb, B. C. Binding Hydrated Anions with Hydrophobic Pockets. *J. Am. Chem. Soc.* **138**, 48–51 (2016).
22. Sullivan, M. R., Yao, W., Tang, D., Ashbaugh, H. S. & Gibb, B. C. The Thermodynamics of Anion Complexation to Nonpolar Pockets. *J. Phys. Chem. B* **122**, 1702–1713 (2018).
23. Rankin, B. M. & Ben-Amotz, D. Expulsion of Ions from Hydrophobic Hydration Shells. *J. Am. Chem. Soc.* **135**, 8818–8821 (2013).

24. Balos, V., Kim, H., Bonn, M. & Hunger, J. Dissecting Hofmeister Effects: Direct Anion–Amide Interactions Are Weaker than Cation–Amide Binding. *Angew. Chem. Int. Ed.* **55**, 8125–8128 (2016).
25. Long, F. A. & McDevit, W. F. Activity Coefficients of Nonelectrolyte Solutes in Aqueous Salt Solutions. *Chem. Rev.* **51**, 119–169 (1952).
26. Stillinger, F. H. Structure in Aqueous Solutions of Nonpolar Solutes from the Standpoint of Scaled-Particle Theory. *J. Solution. Chem.* **2**, 141–158 (1973).
27. Chandler, D. Interfaces and the Driving Force of Hydrophobic Assembly. *Nature* **437**, 640–647 (2005).
28. Davis, J. G., Gierszal, K. P., Wang, P. & Ben-Amotz, D. Water Structural Transformation at Molecular Hydrophobic Interfaces. *Nature* **491**, 582–585 (2012).
29. Hande, V. R. & Chakrabarty, S. Structural Order of Water Molecules around Hydrophobic Solutes: Length-Scale Dependence and Solute–Solvent Coupling. *J. Phys. Chem. B* **119**, 11346–11357 (2015).
30. Pierce, V., Kang, M., Aburi, M., Weerasinghe, S. & Smith, P. E. Recent Applications of Kirkwood-Buff Theory to Biological Systems. *Cell Biochem. Biophys.* **50**, 1–22 (2008).
31. Knowles, D. B. *et al.* Chemical Interactions of Polyethylene Glycols (PEGs) and Glycerol with Protein Functional Groups: Applications to Effects of PEG and Glycerol on Protein Processes. *Biochemistry* **54**, 3528–3542 (2015).
32. Fega, K. R., Wilcox, A. S. & Ben-Amotz, D. Application of Raman Multivariate Curve Resolution to Solvation-Shell Spectroscopy. *Appl. Spectrosc.* **66**, 282–288 (2012).
33. Walrafen, G. E., Fisher, M. R., Hokmabadi, M. S. & Yang, W. -H. Temperature Dependence of the Low- and High-Frequency Raman Scattering from Liquid Water. *J. Chem. Phys.* **85**, 6970–6982 (1986).
34. D'Arrigo, G., Maisano, G., Mallamace, F., Migliardo, P. & Wanderlingh, F. Raman Scattering and Structure of Normal and Supercooled Water. *J. Chem. Phys.* **75**, 4264–4270 (1981).
35. Sun, Q. Local Statistical Interpretation for Water Structure. *Chem. Phys. Lett.* **568–569**, 90–94 (2013).

36. Harada, Y. *et al.* Probing the OH Stretch in Different Local Environments in Liquid Water. *J. Phys. Chem. Lett.* **8**, 5487–5491 (2017).
37. Morawietz, T. *et al.* The Interplay of Structure and Dynamics in the Raman Spectrum of Liquid Water over the Full Frequency and Temperature Range. *J. Phys. Chem. Lett.* **9**, 851–857 (2018).
38. Duboué-Dijon, E. & Laage, D. Characterization of the Local Structure in Liquid Water by Various Order Parameters. *J. Phys. Chem. B* **119**, 8406–8418 (2015).
39. Mackay, D. & Shiu, W. Y. A Critical Review of Henry's Law Constants for Chemicals of Environmental Interest. *J. Phys. Chem. Ref. Data* **10**, 1175–1199 (1981).
40. Meyer, D. E. & Chilkoti, A. Quantification of the Effects of Chain Length and Concentration on the Thermal Behavior of Elastin-like Polypeptides. *Biomacromolecules* **5**, 846–851 (2004).
41. Lee, C., McCammon, J. A. & Rossky, P. J. The Structure of Liquid Water at an Extended Hydrophobic Surface. *J. Chem. Phys.* **80**, 4448–4455 (1984).
42. Lum, K., Chandler, D. & Weeks, J. D. Hydrophobicity at Small and Large Length Scales. *J. Phys. Chem. B* **103**, 4570–4577 (1999).
43. Laage, D., Stirnemann, G. & Hynes, J. T. Why Water Reorientation Slows without Iceberg Formation around Hydrophobic Solutes. *J. Phys. Chem. B* **113**, 2428–2435 (2009).
44. Petersen, C., Tielrooij, K.-J. & Bakker, H. J. Strong Temperature Dependence of Water Reorientation in Hydrophobic Hydration Shells. *J. Chem. Phys.* **130**, 214511 (2009).
45. Xi, E. *et al.* Hydrophobicity of Proteins and Nanostructured Solutes is Governed by Topographical and Chemical Context. *Proc. Natl. Acad. Sci. U.S.A.* **114**, 13345–13350 (2017).
46. Li, I. T. S. & Walker, G. C. Signature of Hydrophobic Hydration in a Single Polymer. *Proc. Natl. Acad. Sci. U.S.A.* **108**, 16527–16532 (2011).
47. Hippel, P. H. von & Wong, K.-Y. On the Conformational Stability of Globular Proteins. The Effects of Various Electrolytes and Nonelectrolytes on the Thermal Ribonuclease Transition. *J. Biol. Chem.* **240**, 3909–3923 (1965).

48. Hwang, T. L. & Shaka, A. J. Water Suppression That Works. Excitation Sculpting Using Arbitrary Wave-Forms and Pulsed-Field Gradients. *J. Magn. Reson. A* **112**, 275–279 (1995).
49. Lee, H., Venable, R. M., MacKerell, A. D. & Pastor, R. W. Molecular Dynamics Studies of Polyethylene Oxide and Polyethylene Glycol: Hydrodynamic Radius and Shape Anisotropy. *Biophys. J.* **95**, 1590–1599 (2008).
50. Chudoba, R., Heyda, J. & Dzubiella, J. Temperature-Dependent Implicit-Solvent Model of Polyethylene Glycol in Aqueous Solution. *J. Chem. Theory Comput.* **13**, 6317–6327 (2017).
51. Berendsen, H. J. C., Grigera, J. R. & Straatsma, T. P. The Missing Term in Effective Pair Potentials. *J. Phys. Chem.* **91**, 6269–6271 (1987).
52. Heyda, J., Vincent, J. C., Tobias, D. J., Dzubiella, J. & Jungwirth, P. Ion Specificity at the Peptide Bond: Molecular Dynamics Simulations of N-Methylacetamide in Aqueous Salt Solutions. *J. Phys. Chem. B* **114**, 1213–1220 (2010).
53. Křížek, T. *et al.* Electrophoretic Mobilities of Neutral Analytes and Electroosmotic Flow Markers in Aqueous Solutions of Hofmeister Salts. *Electrophoresis* **35**, 617–624 (2014).
54. Abraham, M. J. *et al.* GROMACS: High Performance Molecular Simulations through Multi-Level Parallelism from Laptops to Supercomputers. *SoftwareX* **1–2**, 19–25 (2015).
55. Bussi, G., Donadio, D. & Parrinello, M. Canonical Sampling Through Velocity Rescaling. *J. Chem. Phys.* **126**, 14101 (2007).
56. Parrinello, M. & Rahman, A. Polymorphic Transitions in Single Crystals: a New Molecular Dynamics Method. *J. Appl. Phys.* **52**, 7182–7190 (1981).
57. Essmann, U. *et al.* A Smooth Particle Mesh Ewald Method. *J. Chem. Phys.* **103**, 8577–8593 (1995).
58. Hess, B. P-LINCS: A Parallel Linear Constraint Solver for Molecular Simulation. *J. Chem. Theory Comput.* **4**, 116–122 (2008).
59. Paterová, J. *et al.* Reversal of the Hofmeister Series: Specific Ion Effects on Peptides. *J. Phys. Chem. B* **117**, 8150–8158 (2013).

60. Errington, J. R. & Debenedetti, P. G. Relationship between Structural Order and the Anomalies of Liquid Water. *Nature* **409**, 318–321 (2001).